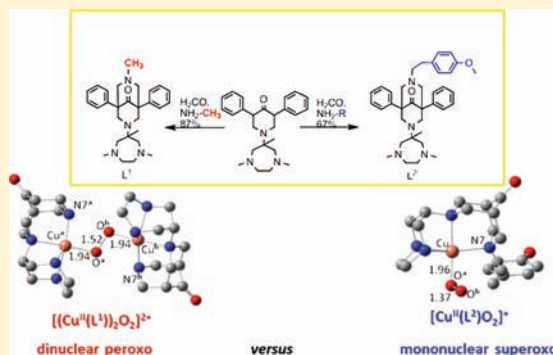


Dioxygen Reactivity of New Bispidine-Copper Complexes

Peter Comba,^{*,†} Christina Haaf,[†] Stefan Helmle,[†] Kenneth D. Karlin,^{*,‡} Shanthi Pandian,[†] and Arkadius Waleska[†][†]Anorganisch-Chemisches Institut, Universität Heidelberg, INF 270, D-69120 Heidelberg, Germany[‡]Department of Chemistry, The Johns Hopkins University, Baltimore, Maryland 21218, United States

S Supporting Information

ABSTRACT: The reactivity of copper complexes of three different second-generation bispidine-based ligands (bispidine = 3,7-diazabicyclo[3.3.1]nonane; mono- and bis-tetradentate; exclusively tertiary amine donors) with dioxygen [(reversible) binding of dioxygen by copper(I)] is reported. The UV–vis, electropray ionization mass spectrometry, electron paramagnetic resonance, and vibrational spectra (resonance Raman) of the dioxygen adducts indicate that, depending on the ligand and reaction conditions, several different species (mono- and dinuclear, superoxo, peroxy, and hydroperoxy), partially in equilibrium with each other, are formed. Minor changes in the ligand structure and/or experimental conditions (solvent, temperature, relative concentrations) allow switching between the different forms. With one of the ligands, an end-on peroxodicopper(II) complex and a mononuclear hydroperoxocopper(II) complex could be characterized. With another ligand, reversible dioxygen binding was observed, leading to a metastable superoxocopper(II) complex. The amount of dioxygen involved in the reversible binding to Cu^I was determined quantitatively. The mechanism of dioxygen binding as well as the preference of each of the three ligands for a particular dioxygen adduct is discussed on the basis of a computational (density functional theory) analysis.



■ INTRODUCTION

A broad range of aerobic oxidation reactions are catalyzed by copper enzymes and low-molecular-weight model complexes. A number of catalytically relevant mono- and dinuclear [CuO₂]ⁿ⁺ and [Cu₂O₂]²⁺ species have been identified and thoroughly studied spectroscopically, structurally, with computational methods, and in terms of their reactivity. Apart from the various types of oxygen adducts (dioxygen, superoxo, peroxy, and oxo) and copper in different oxidation states (Cu^I, Cu^{II}, and Cu^{III}), it is particularly the [Cu₂O₂]²⁺ core that has attracted much attention, specifically in terms of the various possible isomers [bis(μ-oxo), μ-η²:η²-peroxy, and *trans*-μ-1,2-peroxy].^{1–9} The suitability of copper for the activation of dioxygen derives from the favorable redox potentials, tunable over a broad range by the coordination geometry and donor sets. A large variety of ligand systems are known and serve as a valuable basis for biomimetic copper chemistry;^{4–8,10,11} the reactivity and stability ranges depend on the geometry enforced and the donor set provided by the ligand. Structure–activity correlations have been established and are used to modulate the properties of the copper center in order to establish mimics for specific natural systems for electron transfer, dioxygen transport, oxidation, or oxygenation reactivity.

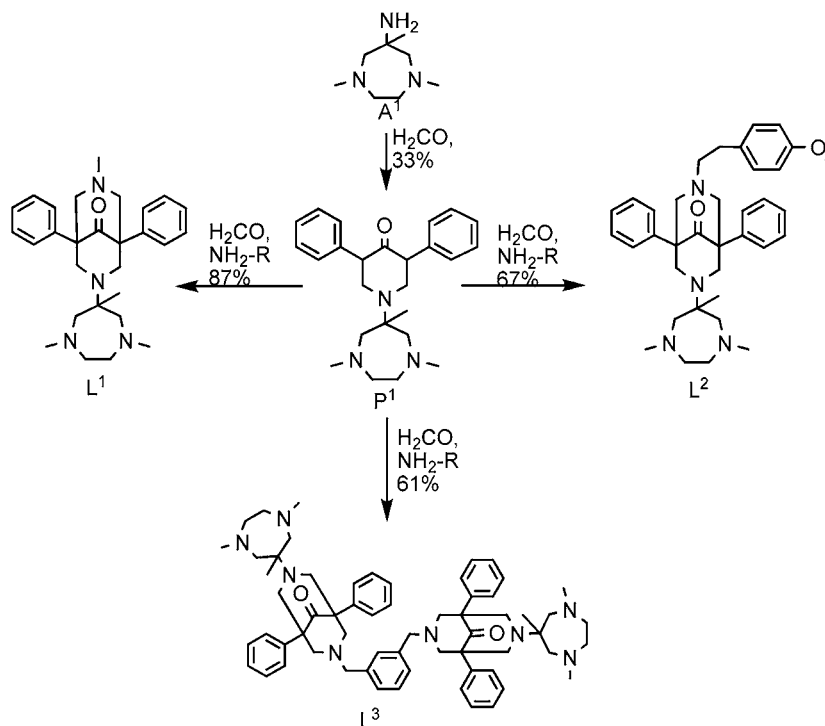
The copper–dioxygen chemistry of a range of bi-, tri-, and tetradentate amine-, imine-, and pyridine-containing ligands are, in the area of copper-based oxygen activation, well-established tris(methylpyridine)amine (tmpa), 1,4,7-triazacyclononane

(tacn), hydrotripyrzylborate, tris(ethylamino)ethane (tren), β-diketiminato ligands, and their derivatives. In particular also the “superbasic” tetramethylguanidino-substituted amine ligands, has led to exciting discoveries, and this has been reviewed extensively.^{9,11,12} The transition-metal coordination chemistry of a large range of tetra-, penta-, and hexadentate bispidine (3,7-diazabicyclo[3.3.1]nonane) ligands started to attract the attention of coordination chemists less than a decade ago, although the first bispidine derivatives were described by Mannich.^{13–16} The first-generation bispidine ligands have mixed aliphatic/aromatic nitrogen-donor sets and enforce distorted *cis*-octahedral coordination geometries; the corresponding copper complexes have been shown to provide interesting enzyme models and efficient catalysts.^{17–22} Of particular interest for the copper–dioxygen chemistry is the fact that the enforced square-pyramidal geometry with an axial amine and in-plane coordination of the substrate (i.e., the dioxygen-derived ligand) leads to an unusual stability of the peroxy complexes,^{17,18,20,21} specific reactivities^{19,23} and interesting spectroscopic properties.^{21,24}

In the recently introduced second-generation bispidine ligands with pure aliphatic donor sets,^{16,25} very different, i.e., distorted trigonal, structures (trigonal bipyramidal or trigonal prismatic) are enforced, and this has important consequences

Received: September 2, 2011

Published: February 14, 2012

Scheme 1. Syntheses and Structures of the Ligands L¹, L², and L³

Syntheses: R=methylamine for L¹ [L^{1A} (model (i) for DFT calculations): all 3 NMe groups are replaced by NH];
 R=2-(4-methoxyphenyl)ethaneamine for L²;
 R=1,3-phenylenedimethaneamine for L³.

for the electronic properties and therefore also for the complex reactivity and stability. Three of these new types of bispidine ligands (L¹, L², and L³ in Scheme 1) and their copper–dioxygen chemistry are discussed in the present report.

RESULTS AND DISCUSSION

1. Synthesis of the Ligands and Complexes. The tetradentate ligand L¹ has been described before.^{16,25} L¹ as well as the tetradentate derivative L² and the dinucleating bis-tetradentate ligand L³ are derived from the known piperidine precursor P¹ (Scheme 1);²⁵ formaldehyde and 4-methoxyphenylethaneamine for L² and *m*-xylenediamine for L³ are the “locking groups”, which, after basic extraction with diethyl ether, produce ligands as pure solids in reasonably good yields.

The copper(I) complexes of L¹, L², and L³ were obtained from [Cu^I(CH₃CN)₄][B(C₆F₅)₄]²⁶ and the ligands in dioxygen-free tetrahydrofuran (THF), containing several drops of acetonitrile (MeCN) to stabilize the resulting Cu^I cation; *n*-pentane was used to precipitate the complexes. It was not possible to isolate and fully characterize the Cu^IL¹ complex as a solid, even with CO used as an electron-withdrawing coligand, which might confer extra stability. This is probably due to the aliphatic nitrogen-donor set and the specific coordination geometry, which stabilize the oxidized form [the stability of the corresponding copper(II) complex has been determined and found to be relatively high].¹⁶ In contrast, the yellow solid of the dinuclear complex [Cu^I₂(L³)]₂[B(C₆F₅)₄]₂ was stable for several days, and it was also characterized in solution by ¹H NMR spectroscopy. A powder of the mononuclear complex [Cu^I(L²)]₂[B(C₆F₅)₄], obtained by the addition of *n*-pentane to the reaction mixture, shows the first signs of decomposition after a few hours. In a CO atmosphere

during the synthesis, a significantly more stable CO-substituted complex is obtained, and this was used for characterization by ¹H NMR and IR spectroscopies. Copper(II) complexes of L² and L³ were obtained in good yield (60–70%) by the reaction of stoichiometric amounts of the ligands and Cu^{II} salts in MeCN (see the Experimental Section), the corresponding L¹-based copper(II) complex has been fully characterized, and the X-ray structure has been reported.^{16,25}

2. Solution Properties of the Copper Compounds. A slight broadening of the signals in the ¹H NMR spectra of [Cu^I(L²)(CO)][B(C₆F₅)₄] and [Cu^I₂(L³)]₂[B(C₆F₅)₄]₂ probably results from slow oxidation of the Cu^I complexes in solution. As expected from the rigid ligand cavity and earlier structural analyses,^{16,25} no isomerism in the ligand binding mode is apparent.²¹ The vibrational frequency of the carbonyl group in the IR spectrum of [Cu^I(L²)(CO)][B(C₆F₅)₄] is at 2100 cm⁻¹, i.e., in the expected range for end-on coordination of CO to Cu^I.^{27,28}

The structures of first-row transition-metal complexes with tetra- and pentadentate second-generation bispidine complexes are best described as distorted trigonal bipyramidal (tbp).^{16,25} Because of the relatively small N–Cu–N angle, enforced by the diazaheptane cycle, the copper(II) complexes have a “d_{x²-y²} ground state” (i.e., the unpaired electron is in d_{x²-y²}; in axial tbp symmetry, the unpaired electron instead is in d_{z²}), and this is reflected in their electron paramagnetic resonance (EPR) spectra.²⁹ That of [Cu^{II}(L²)(OH₂)]²⁺ is very similar to the spectrum of the L¹-based bispidine-copper(II) complex (see Table 1). The electronic spectra of [Cu^{II}(L²)(OH₂)]²⁺ and [Cu^{II}₂(L³)(solvent)₂]⁴⁺ in MeCN have the expected dd transitions at approximately 600 nm; however, the low-energy transition, due to splitting of the e_g set of orbitals (in O_h) in an

Table 1. EPR Parameters of the Copper(II) Complexes [in MeCN/Toluene or MeOH, 90 K; X-Band Frequencies (Approximately 9 GHz)]^a

complex	g_{\parallel}	g_{\perp}	A_{\parallel} [10^{-4} cm ⁻¹]	A_{\perp} [10^{-4} cm ⁻¹]
[Cu ^{II} (L ¹)(NCCH ₃)] ²⁺ ¹⁶	2.21	2.08	170	15
[Cu ^{II} (L ²)(OH)] ⁺	2.22	2.05	170	15

^aThe spin Hamiltonian parameters are determined by spectral simulation with XSophe (the spectra and simulations are given as the Supporting Information).

axial field, was not resolved for the L²- and L³-based complexes (Table 2).

Table 2. UV–Vis–Near-IR Spectral Data of the Copper(II) Complexes at Ambient Temperature in MeCN

complex	λ_1 [nm]/ ϵ [l/(mol·cm)]	λ_2 [nm]/ ϵ [l/(mol·cm)]
[Cu ^{II} (L ¹)(NCCH ₃)] ²⁺ ¹⁶	903/341	627/684
[Cu ^{II} (L ²)(OH ₂)] ²⁺		633/136
[Cu ^{II} ₂ (L ³)] ⁴⁺		599/248

Electrochemical measurements in MeCN indicate for [Cu^{II}(L²)(OH₂)]²⁺ an irreversible reduction at −270 mV (vs SCE, Table 3). This potential is significantly more positive than

Table 3. Cyclic Voltammetry (CV) Data of the Second-Generation Bispidinecopper Compounds in MeCN, 0.1 M (Bu₄N)(PF₆), $E_{1/2}$ vs SCE

complex	$E_{1/2}$ [mV]
[Cu ^{II} (L ¹)(NCMe)] ²⁺	−377
[Cu ^{II} (L ²)(OH ₂)] ²⁺	−270
[Cu ₂ ^{II} (L ³)(solvent) ₂] ⁴⁺	−396 (red), −697 (red), −555 (ox)

that of [Cu^{II}(L¹)(NCMe)]²⁺ (−377 mV) and suggests a higher stability of the copper(I) complex of L² compared to that of L¹.²⁹ For the dinuclear complex [Cu^{II}₂(L³)(solvent)₂]⁴⁺, two reduction peaks and one oxidation peak are observed (see the Supporting Information for the electrochemical traces). This suggests an interaction between the two Cu^I cations in the dinuclear complex, followed by ready decomposition of the dicopper(I) complex.

a. Oxygenation Experiments. *Oxygenation of the Copper(I) Complex with L¹.* *Time-Resolved UV–Vis Spectroscopy.* The tetradentate ligand L¹ forms copper(I) complexes with rich oxygenation reactivity. For the oxygenation experiments, [Cu^I(L¹)]⁺ was synthesized in situ³⁰ by the addition of a [Cu^I(MeCN)₄][B(C₆F₅)₄] solution in a strictly oxygen-free atmosphere to a solution of L¹ in the desired solvent and with the required concentrations. At low temperature (−80 °C) in acetone, a deep-blue species is generated by bubbling molecular oxygen through the in situ generated complex (see Figure 1); identical spectra are observed in the concentration range from 2.5×10^{-4} to 2×10^{-3} M. The spectrum of the oxygenated species (see Figure 1) is dominated by a band at 618 nm with higher energy shoulders at about 520 and 450 nm. These features are in the region where UV–vis transitions of *trans*- μ -1,2-peroxodicopper(II) compounds are observed, such as in the well-characterized [(Cu^{II}(Me₆tren))₂(O₂)]²⁺^{30,31} and [(Cu^{II}(tmpa))₂(O₂)]²⁺^{32,33} systems. However, the intensity ratios in the L¹-based bispidine

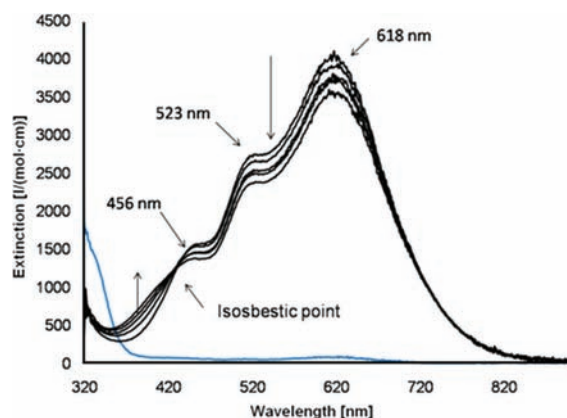


Figure 1. Oxygenation of [Cu^I(L¹)]⁺[B(C₆F₅)₄] (acetone, $T = -80$ °C, 2.5×10^{-4} M), recorded within 105 min. Color code: blue (for comparison), [Cu^I(L¹)]⁺; black, oxygenated complex. The values for extinction coefficients are based on 100% conversion.

system are different from those usually observed for end-on peroxodicopper(II) complexes with local Cu^{II} tbp coordination,^{30,31} and this presumably is due to the unusual coordination geometry enforced by the second-generation bispidine ligands (see the description of the structures above). In fact, such a pattern of charge-transfer (CT) bands with “reversed intensity ratios” was shown to occur in end-on peroxodicopper(II) complexes with ligands that favor local axial Cu^{II} symmetry, i.e., with a $d_{x^2-y^2}$ ground state.^{34,35} The end-on peroxy complex [(Cu^{II}(L¹))₂(O₂)]²⁺, with 618, 520, and 450 nm absorptions, appears to slowly isomerize to another similar species, suggested to be a conformer (see below). The isosbestic point at 420 nm indicates a clean monophasic transformation.

An intensely green solution is obtained at −120 °C in 2-methyltetrahydrofuran (MeTHF; see the Supporting Information for the spectra). In addition to the two bands at 613 and 515 nm, assigned to *trans*-[(Cu^{II}(L¹))₂(O₂)]²⁺, there is a strong additional transition in this solvent at 452 nm, which we assign to [Cu^{II}(L¹)(O₂)]⁺, i.e., a mononuclear η^1 -superoxocopper(II) complex (a similar spectrum is obtained in THF; see the Supporting Information). Moreover, there is another new transition at 340 nm, which is due to a third species, probably a hydroperoxy complex ([Cu^{II}(L¹)(OOH)]⁺; a species with a similar spectrum is observed in diethyl ether; see the Supporting Information). This putative hydroperoxy complex forms relatively slowly (see below for further characterization of this species).

Computational Analysis. Density functional theory (DFT) calculations were performed to confirm the existence of the proposed mono- and dinuclear complexes as oxygenation products of [Cu^I(L¹)]⁺. There is a relatively large body of published computational work, especially on the theoretically challenging dinuclear systems with Cu₂O₂ “diamond” cores,^{36–46} and much of this has recently been reviewed.⁹ Apart from the general problem of choosing the appropriate functional,⁴⁷ the electron distribution in the “diamond” core as a function of the ligand-enforced structure clearly varies with the theoretical method used.^{9,43,44} All spin states were considered, and the structural parameters as well as the relative stabilities are based on the widely tested and used setup involving the B3LYP functional and a triple- ζ basis set (for details, see the Experimental Section; the energies reported

Table 4. Key Structural Parameters and Spin Densities for Various Oxygenated Copper Complexes Involving the Bispidine Ligand L^1 (Lowest-Energy Conformations and Spin States, Where Appropriate; See the Text)

complex	interatomic distances [Å]			spin densities		
	Cu–O	O–O	Cu–N _{avg}	Cu	O	O
$[(Cu^{II}(L^{1A}))_2(O_2)]^{2+}$	1.938, 1.939	1.516	2.193	0.49, –0.49	0.18	–0.18
$[Cu^{II}(L^1)(O_2)]^+$	1.970	1.360	2.147	0.45	0.17	–0.55
$[Cu^{II}(L^1)(O_2H)]^+$	1.911	1.530	2.403	0.50	0.22	–0.01

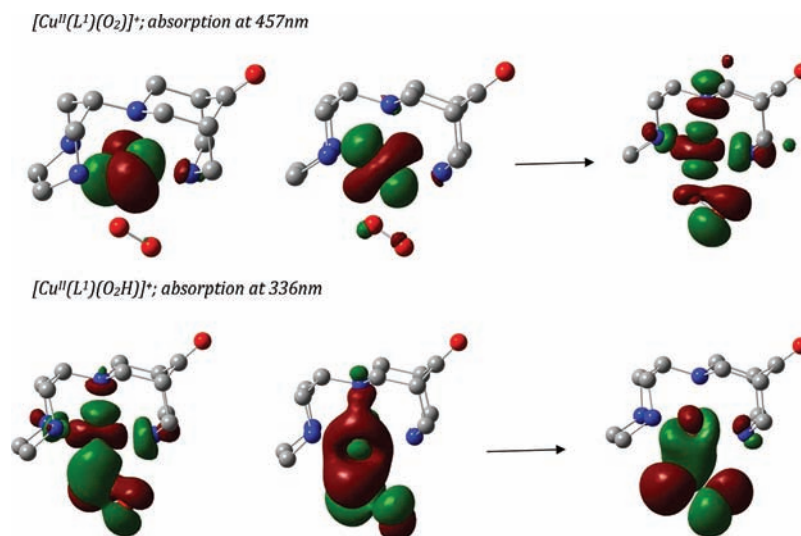


Figure 2. Orbitals involved in the major transitions of the mononuclear complexes.

include corrections for zero-point energies and solvation). The electronic transitions for the various complexes were calculated with ab initio methods and time-dependent DFT (TDDFT), except for the dinuclear complex, for which, because of the larger size of the model, only a TDDFT analysis was performed. Two models were used for the computation of this complex; (i) the terminal methyl groups of the three nitrogen donors (see Scheme 1) were replaced by hydrogen atoms in $[(Cu^{II}(L^{1A}))_2(O_2)]^{2+}$; (ii) the methyl groups were modeled to allow possible interactions of the methyl hydrogen atoms with the O–O bridge of $[(Cu^{II}(L^1))_2(O_2)]^{2+}$. The optimized structural parameters and spin densities for the lowest-energy structure of the *trans*- $[(Cu^{II}(L^{1A}))_2(O_2)]^{2+}$ complex are listed in Table 4, together with the corresponding data for the mononuclear superoxo and the hydroperoxo complexes. All possible spin states and different orientations of the peroxo and superoxo groups (end-on or side-on) were considered, and the relative energies and spin densities are given in the Supporting Information.

The dinuclear *trans*- $[(Cu^{II}(L^{1A}))_2(O_2)]^{2+}$ complex was modeled with three different configurations of the O–O bridge, i.e., end-on *trans*-peroxo, side-on (μ - η^2 - η^2) peroxo, and bis(μ -oxo). Only the *trans*- μ -1,2-peroxo (end-on) structure was found to be stable; the other two collapsed upon optimization to the stable isomer. Possible spin states for the *trans*- $[(Cu^{II}(L^{1A}))_2(O_2)]^{2+}$ complex were then considered. The open-shell singlet and triplet states are relatively close in energy (7.5 kJ/mol in favor of the singlet state). This indicates that the dicopper(II) complex has a diamagnetic ground state, and antiferromagnetic coupling of the two Cu^{II} centers is also evident from their spin densities (see Table 4). Single-point calculations with a larger basis and inclusion of the solvent (B2) predict the two spin states to be even closer in energy, i.e., just

differing by 1.8 kJ/mol. TDDFT calculations of the dinuclear *trans*- $[(Cu^{II}(L^{1A}))_2(O_2)]^{2+}$ complex yield peaks of higher intensity at 580, 530, and 490 nm and a peak with very low intensity around 670 nm; this is in acceptable agreement with the experimental absorptions at 620, 520, and 460 nm (see, e.g., Figure 1).⁴⁸ These peaks are characteristic for CT transitions. According to the DFT calculations, the absorptions at 580 and 530 nm correspond to the usual π^* -to-Cu CT transitions involving the peroxo group and the two Cu^{II} centers, and the lower intensity peak at 490 nm is assigned to be due to ligand-to-metal CT (LMCT) transitions (see the Supporting Information).

As mentioned, compared to most other known *trans*- μ -peroxodicopper complexes, the experimentally observed absorption spectrum of *trans*- $[(Cu^{II}(L^1))_2(O_2)]^{2+}$ is significantly different with respect to the intensities, and the TDDFT-predicted transition energies are not as accurate as one might have hoped. Therefore, TDDFT calculations were also performed for the known dinuclear *trans*- μ -peroxo-Cu-tmpa complex. That absorption spectrum has a more intense peak at 530 nm and a less intense transition at 604 nm.^{32,33} The calculated spectrum of the dinuclear peroxo-Cu-tmpa complex has the highest intensity peak at 567 nm, in reasonable agreement with the experimental value, within the limits of the method used. Further low-intensity signals were found at 550, 530, and 507 nm.

The direct reaction of O_2 with $[Cu(L^1)]^+$ results in a mononuclear superoxocopper(II) complex, but a mononuclear peroxocopper(II) complex may also emerge from further reactions (see also the experimental observations above); the peroxide and superoxide moieties can be bound in side-on or end-on orientations. The calculations predict that the superoxo complex is favored by 8.0 kJ/mol over the peroxo complex.

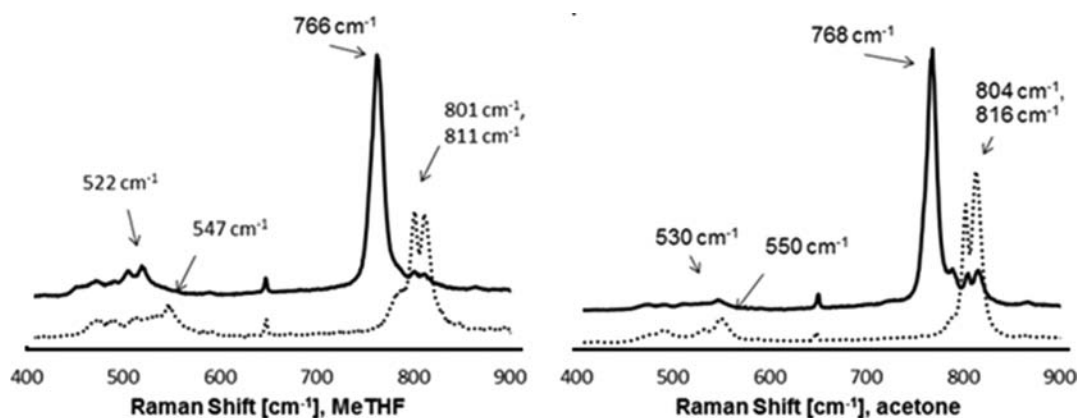


Figure 3. rR spectra of the product of oxygenation of $[\text{Cu}^{\text{I}}(\text{L}^1)]^+$ in MeTHF (left) and acetone (right), -80°C , $c = 22 \times 10^{-3} \text{ M}$, $\lambda_{\text{laser}} = 623 \text{ nm}$: full line, $^{18}\text{O}_2$; dotted line, $^{16}\text{O}_2$.

This is mainly due to the change in the electronic configuration at the Cu^{II} center.⁴⁹ The side-on configuration of the superoxo complex of $[\text{Cu}^{\text{II}}(\text{L}^1)]^{2+}$ was found to be sterically hindered and reverted to the end-on complex upon optimization. The relative energies of the triplet and open-shell singlet states of the end-on superoxo complex $[\text{Cu}^{\text{II}}(\text{L}^1)(\text{O}_2)]^+$ were found to favor the triplet state by 7.4 kJ/mol (basis set B2). The open-shell singlet state was calculated using the broken-symmetry approach that takes nondynamic correlation effects into account with DFT. TDDFT calculations of the singlet state afforded a peak at 426 nm with the maximum intensity, and this agrees well with the experimentally found range of $\sim 410\text{--}450 \text{ nm}$ (dependent on the solvent used; see the experimental spectra). This supports the mononuclear superoxo species as a product of the oxidation of $[\text{Cu}^{\text{I}}(\text{L}^1)]^+$, as suggested by the low-temperature time-dependent UV–vis spectra. In fact, all of these results are in line with relatively recent findings on structurally related tetradentate tripodal ligands and corresponding η^1 -superoxocopper(II) species formed from their (ligand) $\text{Cu}^{\text{I}}/\text{O}_2$ reactions;^{45,52–54} for example, a triplet $S = 1$ ground state emerges from spectroscopic and computational studies^{45,53} on the X-ray structurally characterized complex $[(\text{tmg}_3\text{tren})\text{Cu}^{\text{II}}\text{O}_2]^+$ (where $\text{tmg}_3\text{tren} = 1,1,1\text{-tris}[2\text{-}[\text{N}^2\text{-}(1,1,3,3\text{-tetramethylguanidino})\text{ethyl}]\text{amine}]$).⁵² Also, the prominent UV–vis spectroscopic features observed for $[\text{Cu}^{\text{II}}(\text{L}^1)(\text{O}_2)]^+$ are very much like those known for other established superoxocopper(II)(ligand) species.^{8,45,53–55}

Because of the relatively small size of the molecules, ab initio calculations were also carried out to calculate the absorption bands of the two mononuclear complexes. The absorption spectrum of the superoxo complex $[\text{Cu}^{\text{II}}(\text{L}^1)(\text{O}_2)]^+$ was calculated with a reference space of (16,9), i.e., with two half-filled orbitals. The SORCI-predicted spectrum has absorption maxima at 457 and 470 nm, in good agreement with the experimentally observed transitions. The absorption at 457 nm is a dd transition (see Figure 2). The TDDFT-calculated value of the transition for the mononuclear end-on hydroperoxo complex $[\text{Cu}^{\text{II}}(\text{L}^1)(\text{OOH})]^+$ is in the range of $\sim 360 \text{ nm}$, which is in good agreement with the experimental spectral range of 340–370 nm. SORCI calculations for this species were performed with a reference space of (19,10). The ab initio calculated spectrum shows maximum-intensity peaks at 336 and 415 nm and therefore supports the analysis discussed above. The major transition involved is a hydroperoxo-to- Cu^{II} LMCT transition; see Figure 2.

Resonance Raman (rR) Spectra of the Oxygenated Copper(I) Complexes with L^1 . For further identification of the oxygenated $[\text{Cu}^{\text{I}}(\text{L}^1)]^+$ complexes, rR spectra were recorded (excitation wavelength of 623 nm, MeTHF or

Table 5. Experimental and Calculated rR Transitions of the Oxygenation Product of $[\text{Cu}^{\text{I}}(\text{L}^1)]^+$ at -80°C (Computed Values Not Scaled; See the Text)

solvent	O–O, $^{16}\text{O}_2$ [cm^{-1}]	Cu–O, $^{16}\text{O}_2$ [cm^{-1}]	O–O, $^{18}\text{O}_2$ [cm^{-1}]	Cu–O, $^{18}\text{O}_2$ [cm^{-1}]	$\Delta(16,18)$ O–O [cm^{-1}]	$\Delta(16,18)$ Cu–O [cm^{-1}]
MeTHF	811, 801	547	766	522	45, 35	25
acetone	816, 804	550	768	530	48, 36	20
calculated	808, 798	495, 495				

acetone, -80°C ; see Figure 3 and Table 5). In MeTHF with $^{16}\text{O}_2$, two bands for the O–O stretching mode are seen at 811 and 801 cm^{-1} , and these shift to one transition at 766 cm^{-1} with $^{18}\text{O}_2$. In acetone, the corresponding bands are at 816 and 804 cm^{-1} with $^{16}\text{O}_2$ and at 768 cm^{-1} with $^{18}\text{O}_2$. The Cu–O vibration in MeTHF is at 547 cm^{-1} ($^{16}\text{O}_2$) and 522 cm^{-1} ($^{18}\text{O}_2$) and the corresponding transition energies in acetone are at 550 cm^{-1} ($^{16}\text{O}_2$) and 530 cm^{-1} ($^{18}\text{O}_2$). These energies are as expected for the O–O and Cu–O modes of *trans- μ -1,2*-peroxocopper(II) adducts⁴ and indicate that the blue species generated in acetone at -80°C (see Figure 1) indeed is a *trans*- $[(\text{Cu}^{\text{II}}(\text{L}^1))_2\text{O}_2]^{2+}$ complex. The presence of two signals for the O–O bridge in natural abundance dioxygen might be the result of torsional isomers. DFT calculations of different torsional isomers support this assumption, and the relative energies are found to vary in a range of approximately 20 kJ/mol. The lowest-energy isomer is shown in Figure 4 and has a dihedral angle of 180° , involving the $\text{N}7^{\text{a}}\text{--Cu}^{\text{a}}\text{--Cu}^{\text{b}}\text{--N}7^{\text{b}}$ centers. This torsional angle was varied to 0° , 30° , 60° , and 90° to find the relative energies of the various conformations. The Cu–O and O–O stretching frequencies, calculated for the two lowest-energy structures (180° and 120°), are presented along with the experimental values in Table 5. The O–O stretching frequencies are in reasonable agreement with the experimental frequencies, but there is some discrepancy with the Cu–O band. Another possible interpretation of the double peaks with the $^{16}\text{O}_2$ and one peak with the $^{18}\text{O}_2$ peroxo complex,

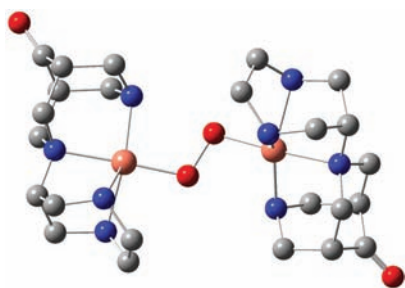


Figure 4. Lowest-energy isomer of the dinuclear *trans*- $[(\text{Cu}^{\text{II}}(\text{L}^1))_2(\text{O}_2)]^{2+}$ complex (hydrogen atoms omitted for clarity; Cu–O = 1.94 Å; O–O = 1.52 Å; see the Supporting Information for details).

independent of the solvent, is the occurrence of a Fermi resonance.^{45,56–58}

EPR Spectra of the Oxygenated Copper(II) Complexes with L^1 . The dinuclear *trans*- $[(\text{Cu}^{\text{II}}(\text{L}^1))_2(\text{O}_2)]^{2+}$ complex is antiferromagnetically coupled (see also the DFT analysis above), and the mononuclear superoxo species $[\text{Cu}^{\text{II}}(\text{L}^1)(\text{O}_2)]^+$ has a triplet ground state. This also emerges from the calculated spin densities of these complexes (see Table 4; there is an energy difference of 11.4 kJ/mol in favor of the triplet relative to the open-shell singlet state for the superoxo complex $[\text{Cu}^{\text{II}}(\text{L}^1)(\text{O}_2)]^+$). Therefore, these complexes are not expected to show EPR transitions at liquid-nitrogen temperatures,⁵³ and indeed frozen solutions of the oxygenated complex in acetone and THF are EPR-silent. However, a frozen solution ($-80\text{ }^\circ\text{C}$) of the oxygenated $[\text{Cu}^{\text{I}}(\text{L}^1)]^+$ complex in MeTHF, where the UV–vis spectra suggested the presence of a mononuclear hydroperoxo complex (see above), shows an EPR signal, with parameters as expected for a mononuclear hydroperoxo complex, $[\text{Cu}^{\text{II}}(\text{L}^1)(\text{OOH})]^+$ (Figure 5 and Table 6; for a dinuclear complex such as *trans*- $[(\text{Cu}^{\text{II}}(\text{L}^1))_2(\text{O}_2)]^{2+}$, a half-field signal would also be expected, and this was not detected here). An additional small signal of a mononuclear copper(II) species, also visible in Figure 5, is assigned to a minor impurity of a copper(II) decay product. As expected for a hydroperoxo complex, the spectrum is well resolved,⁵⁹ and upon warming, the solution exhibits the known pattern for $[\text{Cu}^{\text{II}}(\text{L}^1)]^{2+}$.¹⁶ The quantum-chemically computed *g* and *A* tensor parameters (see above and the Experimental Section) are in good agreement with the experimental values for both the hydroperoxo and MeCN species, which were recorded and computed for comparison (see Table 6).

Reaction Pathways for Oxygenation of the Copper(II) Complex with L^1 . The L^1 -based copper(I) complex has a rich

oxygen activation chemistry. At least three oxygenated species are present, and the reaction pathway depends on the solvent, the relative concentrations, and the temperature (see Scheme 2).

From the spectroscopic data (UV–vis, EPR, and rR) and in combination with the computational characterization, we conclude that at very low temperature and in low concentrations, first an end-on superoxo complex $[\text{Cu}^{\text{II}}(\text{L}^1)(\text{O}_2)]^+$ is formed. In acetone, diethyl ether, or MeTHF at $-80\text{ }^\circ\text{C}$, this reacts in a very fast process to *trans*- $[(\text{Cu}^{\text{II}}(\text{L}^1))_2(\text{O}_2)]^{2+}$, and this is a common pathway.⁴ In THF, the superoxo complex $[\text{Cu}^{\text{II}}(\text{L}^1)(\text{O}_2)]^+$ is longer-lived, and it is also stabilized in MeTHF at $-120\text{ }^\circ\text{C}$. The dinuclear *trans*-peroxo complex $[(\text{Cu}^{\text{II}}(\text{L}^1))_2(\text{O}_2)]^{2+}$ (see Figure 1; acetone solution) decays slowly. In diethyl ether and MeTHF, the *trans*- $[(\text{Cu}^{\text{II}}(\text{L}^1))_2(\text{O}_2)]^{2+}$ species is converted to a mononuclear hydroperoxo complex, $[\text{Cu}^{\text{II}}(\text{L}^1)(\text{OOH})]^+$, which also can be prepared from $[\text{Cu}^{\text{II}}(\text{L}^1)]^{2+}$ and H_2O_2 . Reaction mixtures studied were warmed to ambient temperature, and from those solutions, electrospray ionization mass spectrometry (ESI-MS) spectra were recorded, which reveal $[\text{Cu}^{\text{II}}(\text{L}^1)]^{2+}$ as the main decomposition fragment, and only traces of species with an oxygenated ligand backbone.

b. Oxygenation of the Copper(II) Complex with L^2 . L^2 has a ligand cavity that is identical with that of L^1 , but the ligand has a methoxy-substituted phenyl ring (see Scheme 1) in order to potentially mimic an enzymatic substrate found in close proximity to the $\text{Cu}^{\text{I}}/\text{O}_2$ -derived site. In spite of the seemingly small change in the ligand structure compared to L^1 , the copper(I)–dioxygen chemistry is very different. In view of the observed redox potentials, this is not entirely unexpected (see above and Table 3). As the oxygenation product, only one intensely green species with maxima in the electronic spectra at ca. 400 and 650 nm was found, independent of the solvent (acetone, THF, and MeTHF), temperature (-80 to $-120\text{ }^\circ\text{C}$), and concentration ($c = 2 \times 10^{-4}$ – 2.5×10^{-3} M; see Figure 6).

The UV–vis spectrum is as expected for a mononuclear η^1 -superoxo- $[\text{Cu}^{\text{II}}(\text{L}^2)(\text{O}_2)]^+$ complex;^{4,30} see also above. The clean isosbestic point suggests that this is the only oxygenation product. This is also supported by the fact that the relative intensities of the two bands at 664 and 402 nm do not change [2.1–2.4 (402 nm) to 1 (664 nm)] if the concentration is varied over the range $c = 2 \times 10^{-4}$ – 2.5×10^{-3} M.

The superoxocopper(II) oxygenation product is stable at $-80\text{ }^\circ\text{C}$ for about 24 h. If warmed to room temperature, the color changes from intensely green to very light green. Upon cooling again to $-80\text{ }^\circ\text{C}$, the dark-green color is reproduced; i.e., binding of dioxygen and formation of the mononuclear

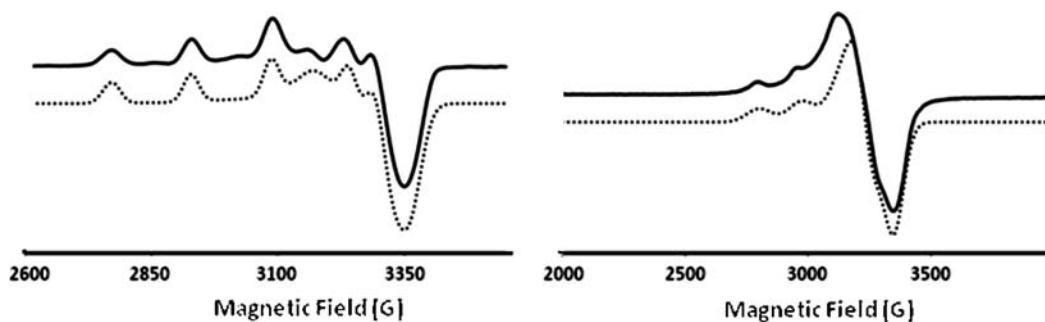


Figure 5. EPR spectrum of $[\text{Cu}^{\text{II}}(\text{L}^1)\text{O}_2\text{H}]^{2+}$ (left) and $[\text{Cu}^{\text{II}}(\text{L}^1)(\text{NCCH}_3)]^{2+}$ (right); frozen solutions (90 K, MeCN/toluene): continuous line, experiment; dashed line, X-Sophe⁶⁴ simulation.

Table 6. Spin Hamiltonian Parameters of the Experimental EPR Spectra (X-Band Frequencies, X-Sophe⁶⁴ Simulation; See Figure 6) (and Calculated Parameters; DFT, See the Text) of $[\text{Cu}^{\text{II}}(\text{L}^1)(\text{O}_2\text{H})]^{2+}$ and $[\text{Cu}^{\text{II}}(\text{L}^1)(\text{NCCH}_3)]^{2+}$

complex	g_x	g_y	g_z	A_x [10^{-4} cm ⁻¹]	A_y [10^{-4} cm ⁻¹]	A_z [10^{-4} cm ⁻¹]
$[\text{Cu}^{\text{II}}(\text{L}^1)(\text{O}_2\text{H})]^{2+}$	2.034 (2.026)	2.074 (2.065)	2.232 (2.137)	31 (27)	33 (33)	162 (168)
$[\text{Cu}^{\text{II}}(\text{L}^1)(\text{NCCH}_3)]^{2+}$	2.08 (2.06)	$g_y = g_x$	2.21 (2.27)	15 (30)	$A_y = A_x$	170 (172)

Scheme 2. Reaction Pathways for Oxygenation of $[\text{Cu}^{\text{I}}(\text{L}^1)]^+$

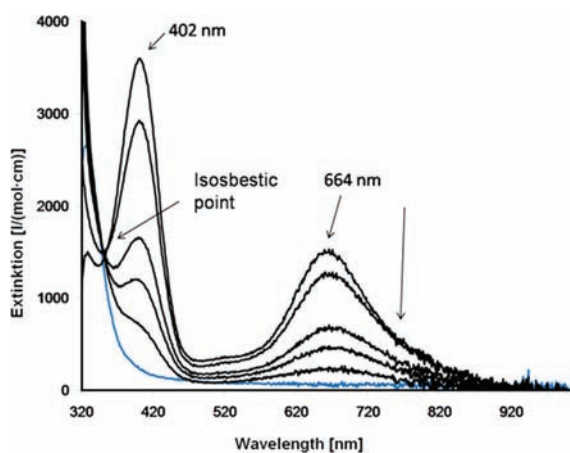
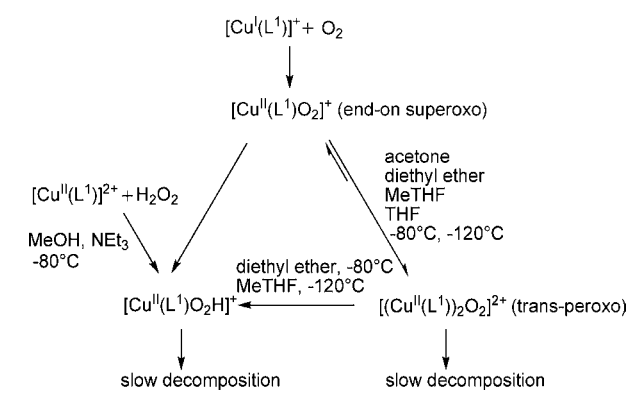


Figure 6. Decay of $[\text{Cu}^{\text{I}}(\text{L}^2)(\text{O}_2)]^+$ (acetone, saturated with O_2 ; -80°C ; $c = 5.0 \times 10^{-4}$ M), recorded over 10 min while warming up to ambient temperature. Color code: blue (for comparison), $[\text{Cu}^{\text{I}}(\text{L}^2)]^+$; black, oxygenated complex. The values for the extinction coefficients are based on 100% conversion of $[\text{Cu}^{\text{I}}(\text{L}^2)]^+ + \text{O}_2 \rightleftharpoons [\text{Cu}^{\text{I}}(\text{L}^2)(\text{O}_2)]^+$.

superoxo complex (temperature-dependent equilibrium) is to a large extent reversible (see Figure 7), and this behavior appears to be the first such example thus far reported. The amount of dioxygen liberated upon warming of the reaction mixture was determined quantitatively with pyrogallol as the indicator (see the Experimental Section):⁶⁰ in a solution of 1.0×10^{-3} mol/L of $[\text{Cu}^{\text{I}}(\text{L}^2)]^+$ (THF, -80°C), the reversibly bound dioxygen is determined to be 75% of the expected amount (see Supporting Information). The decomposition of the L^2 -based superoxo complex $[\text{Cu}^{\text{II}}(\text{L}^2)(\text{O}_2)]^+$ was also followed spectrophotometrically (THF, -35°C), and the resulting half-life time is $t_{1/2} = 30$ min. Figure 8 shows a first-order decay kinetic trace, and this emphasizes the existence of only one oxygenation product (i.e., the superoxo complex), which decomposes to $[\text{Cu}^{\text{II}}(\text{L}^2)]^{2+}$. This is further supported by ESI-MS spectrometry, where $[\text{Cu}^{\text{II}}(\text{L}^2)]^{2+}$ was detected as the main decomposition product.

DFT calculations on the superoxo complex $[\text{Cu}^{\text{II}}(\text{L}^2)(\text{O}_2)]^+$ were performed, and it was found that the triplet state with an

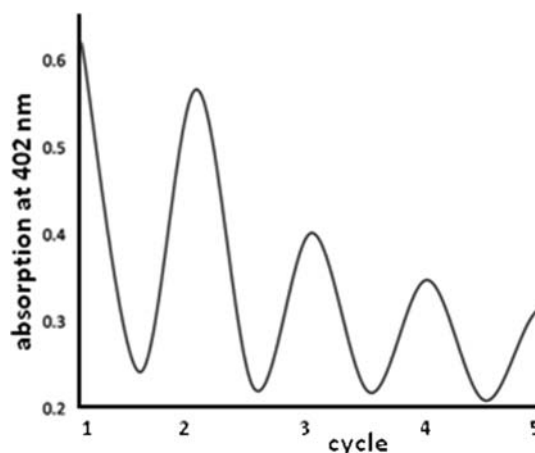


Figure 7. Cycles of $[\text{Cu}^{\text{II}}(\text{L}^2)(\text{O}_2)]^+$ (acetone, saturated with O_2 ; -80°C ; $c = 5.0 \times 10^{-4}$ M) with its decay product $[\text{Cu}^{\text{I}}(\text{L}^2)]^+$, as a function of the temperature (closed vessel, absorption at $\lambda = 402$ nm (see the text). The cycles involve cooling to -80°C (maximum absorption at 402 nm) and warming to ambient temperature within approximately 30 min (minimum absorption at 402 nm).

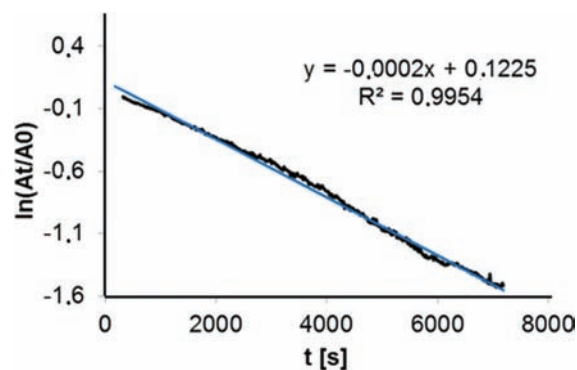


Figure 8. Half-life ($t_{1/2}$) $\ln(A_t/A_0)$ vs t [s], where A_0 = absorption at $t = 0$ s and A_t = absorption at t , of $[\text{Cu}^{\text{II}}(\text{L}^2)(\text{O}_2)]^+$ at -35°C ; THF, $c = 5 \times 10^{-4}$ M; $\lambda = 408$ nm.

end-on orientation is 11.9 kJ/mol lower in energy than the side-on-oriented singlet state.

c. Comparison of the Two Systems Based on Ligands L^1 and L^2 . Although the structural difference between the ligands L^1 and L^2 is small, the copper–dioxygen chemistry is very different. Therefore, the O_2 binding energies between the two systems and the steric hindrance induced by the aromatic moiety upon formation of the dinuclear L^2 -based complex were studied by DFT calculations. The optimized structures of the mononuclear superoxo complexes $[\text{Cu}^{\text{II}}(\text{L}^1)(\text{O}_2)]^+$ and $[\text{Cu}^{\text{II}}(\text{L}^2)(\text{O}_2)]^+$ and of the corresponding dinuclear *trans*-peroxo complexes, together with relevant structural parameters, are shown in Figure 9. Similar to the mononuclear L^1 -based superoxo complex, the triplet and open-shell singlet species are relatively close in energy for the L^2 -based system. The strain accompanying the formation of the dinuclear *trans*-peroxo- $[(\text{Cu}^{\text{II}}(\text{L}^1))_2(\text{O}_2)]^{2+}$ complex was calculated by modification of

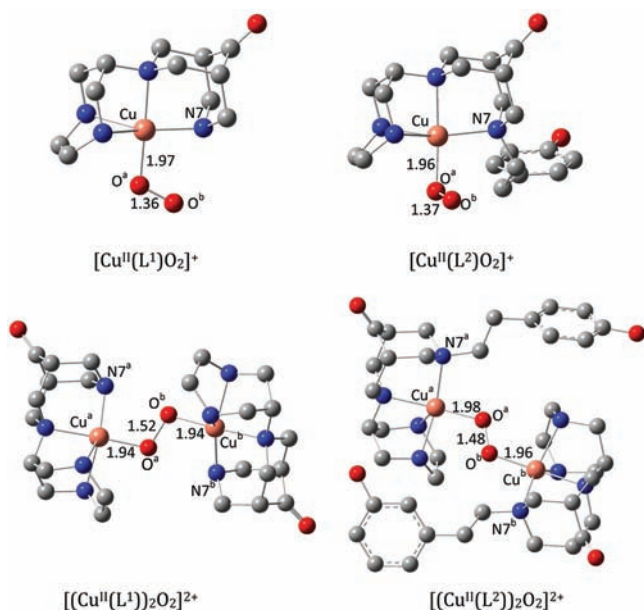


Figure 9. DFT-optimized geometries and key structural parameters of the mono- and dinuclear copper(II)-dioxygen complexes with L^1 and L^2 (hydrogen atoms are omitted for clarity).

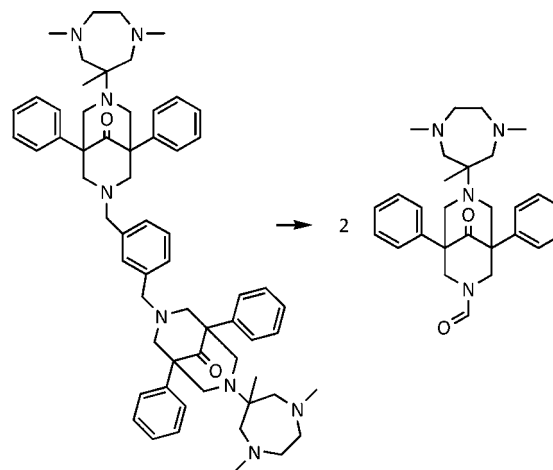
the optimized $[(Cu^{II}(L^2))_2(O_2)]$ complex to yield the corresponding L^1 -based dicopper(II) species, followed by a single-point calculation. The resulting approximate strain energy for formation of the dinuclear peroxo complex $[(Cu^{II}(L^2))_2(O_2)]^{2+}$, induced by the N7-based substituent in L^2 , is 79.8 kJ/mol. A considerable strain also emerges from the optimized geometry of the dinuclear L^2 - in comparison to the L^1 -based complex shown in Figure 9: the slightly elongated Cu–O distances (0.02–0.04 Å) for the L^2 -based complex compared to that of the L^1 -based system reveals the steric hindrance that may prevent the ready formation of the dinuclear complex. In addition, the binding of superoxide and peroxide to mono- and dinuclear $Cu^{II}(L^1)$ and $Cu^{II}(L^2)$ complexes were compared: in the mononuclear case, formation of the end-on superoxo- $[Cu^{II}(L^1)(O_2)]^+$ complex is favored over the $[Cu^{II}(L^2)(O_2)]^+$ analogue by 11.1 kJ/mol. Similarly, the peroxo binding energy for the dinuclear species is found to be in favor of the L^1 -based complex by 20.3 kJ/mol. Both findings are largely due to the sterics of the methoxyphenylethyl group and are in agreement with the experimental observations.

d. Oxygenation of the Dicopper(I) Complex with L^3 . The ligand L^3 with its *m*-xylene bridge provides the possibility to form both *trans*-peroxo complexes ($Cu:O_2$ ratio of 2:1) and complexes that are oxygenated at both copper centers ($Cu:O_2$ ratio of 2:2). The electronic spectrum generated at -80 °C in acetone ($c = 1.3 \times 10^{-3}$ M) has two bands at 334 and 406 nm, as well as a weak band at 637 nm (see the Supporting Information). The oxygenation product is not stable; i.e., the band at 406 nm decays within 60 min at -80 °C. The assignment of the spectra to specific oxygenated complexes is not unambiguous.

The UV–vis spectrum of oxygenated $[Cu_2(L^3)]^{2+}$ at -120 °C in MeTHF has three bands at 412, 563, and 678 nm (see the Supporting Information). These electronic transitions are typical for an end-on superoxo complex.⁵⁵ Although the structure of $[Cu_2(L^3)]^{2+}$ allows for both *trans*-peroxo and end-on superoxo, the end-on superoxo complex seems to be

preferred because of the steric strain induced by a potential *trans*-peroxo bridge. After warming to -80 °C, the three bands decrease in intensity, and a new band at 398 nm is formed. This is very similar to the spectrum observed in acetone. A solution of the oxygenated complex (-120 °C) was allowed to warm to ambient temperature and was then analyzed by ESI-MS spectrometry. Interestingly, a partially oxidized ligand was characterized (see the Supporting Information). The main fragment is a bispidine-derived aldehyde, which is proposed to be formed by attack at the CH benzylic position near to the *m*-xylene group (see Scheme 3 and also the Supporting

Scheme 3. Oxidative Decomposition of $[Cu_2(L^3)(O_2)_2]^{2+}$



Information). This is not an unexpected reaction, and similar pathways have been described before.^{55,61–63} However, at this time we cannot be sure about what species is effecting the oxidative N-dealkylation reaction, a superoxo, $(Cu^{II})_2$ -peroxo, or another $[Cu_2(L^3)]^{2+}/O_2$ -derived species.

CONCLUSIONS

The copper(I) complexes of three second-generation bispidine ligands (one of them dinucleating) were oxygenated, and the oxygenation products as well as their formation and decay pathways were studied. Because of the high reactivity of the copper(I) precursors and the intermediates, the characterization of some of the species involved is not unambiguous if taken alone. However, the thorough spectroscopic analysis of some key species as well as their computational analysis leads to a self-consistent overall picture of the systems.

The μ -peroxodicopper(II) complex of the L^1 -based ligand is thoroughly characterized by its time-dependent UV–vis spectra and the resonance Raman transitions with $^{16}O_2$ - and $^{18}O_2$ -labeled peroxo bridges. The computational analysis in this case leads to a better understanding of a few details but primarily serves to validate the theoretical model used. Also well characterized is the mononuclear hydroperoxocopper(II) complex of L^1 , and this is primarily based on the EPR spectrum, which is compared to other $Cu^{II}L^1$ spectra and, importantly, is in good agreement with the computed spectrum. The time-dependent UV–vis spectra support these assignments and show the various pathways for interconversion between the various species. The third species that can be assigned without much speculation is the mononuclear superoxocopper(II) complex of L^2 . The assignment primarily is based on the clean formation equilibrium that only involves two copper-

based species: the copper(I) complex of L^2 and the corresponding superoxocopper(II) complex. This is a clean 1:1 ($Cu^I:O_2$) reaction, and we have shown that it is reversible over many cycles (with a minor amount of decay products formed, as one would expect), and the superoxocopper(II) complex has the expected electronic properties; specifically, its UV–vis spectrum has the expected transitions. On the basis of this assignment of the L^2 -based superoxocopper(II) complex, we are able to also assign the much more reactive L^1 -based superoxocopper(II) complex by its time-dependent UV–vis spectrum; the two structures are very similar to each other (as expected, and supported by the DFT-optimized structures), and the assignment of the L^1 -based superoxo complex is also strongly supported by the computed UV–vis spectra. We therefore believe that all important species in the L^1 - and L^2 -based complexes are part of a self-consistent interpretation with well-characterized key species. The compounds involved in the L^3 -based copper–dioxygen chemistry are not well characterized, and this system is only presented here to show possible pathways and reactivities of these systems. Of specific interest is the very different stabilities/reactivities of the L^1 - and L^2 -based superoxocopper(II) complexes, and it is quite clear that this is a result of efficient shielding of the active site with the L^2 ligand substituent. Small geometric differences, as observed in L^3 , that lead to amine dealkylation support this interpretation and point toward future studies of the reactivities of these superoxo complexes with external substrates.

It is of interest to compare the systems presented here with those based on other ligand systems. The main difference between the first- and second-generation bispidine ligands is in terms of the structures they enforce to the metal ions; clearly, the difference in the donor sets also is of importance, specifically with respect to the redox potentials, which obviously are of importance in terms of oxygen activation: while the first-generation bispidines enforce square-pyramidal geometries with very stable μ -peroxodicopper(II) (in-plane-coordinated peroxy group), the second-generation bispidines lead to distorted *tpb* complexes with an apical peroxy group; note that the ligand-enforced distortion from trigonal symmetry leads to a $d_{x^2-y^2}$ ground state and to a reactivity that strongly differs not only from that of the first-generation bispidine-based systems but also from those of other ligand-copper complexes described in the literature.

EXPERIMENTAL SECTION

Materials and Measurements. Chemicals (Aldrich and Fluka) were used without further purification if not otherwise stated. L^1 and $[Cu^I(L^1)(NCCH_3)](BF_4)_2$ were described before.²⁵ NMR spectra were recorded at 200.13 MHz (1H) and 50.33 MHz (^{13}C) on a Bruker AS-200 or a Bruker DRX-200 instrument with the solvent signals used as references. IR spectra were recorded with a Perkin-Elmer Spectrum 100 FT-IR spectrometer from KBr pellets. Mass spectra were obtained with a JEOL JMS-700 or Finnigan TSQ 700/Bruker ApexQe hybrid 9.4 FT-ICR instrument. Electronic spectra were measured with a Tidas II J&M or a Jasco V-570 UV–vis–near-IR spectrophotometer. EPR measurements were performed on a Bruker ELEXSYS-E-500 instrument at 125 K; spin Hamiltonian parameters were obtained by simulation of the spectra with *XSophe*.⁶⁴ For electrochemical measurements, a BAS-100B Workstation was used, with a three-electrode setup, consisting of a glassy carbon working electrode, a platinum-wire auxiliary electrode, and, for MeCN solutions, an Ag/AgNO₃ reference electrode [0.01 M AgNO₃, 0.1 M (Bu₄N)(PF₆), degassed CH₃CN] and solutions of the complexes in MeCN/0.1 M (Bu₄N)(PF₆); the potential of the Fc⁺/Fc⁻ couple for the MeCN setup had a value of +91 mV (MeCN, scan rate of 100 mV/s).

Elemental analyses were obtained from the analytical laboratories of the chemical institutes at the University of Heidelberg on a Vario EL (Elementary) instrument.

Computational Details. The presence of various oxygenated species upon reaction with each of the three bispidine ligands was supported by theoretical calculations. Geometry optimizations and frequency calculations were carried out using *Jaguar*,⁶⁵ employing the hybrid density functional, B3LYP,^{66,67} and the effective core pseudopotential, LACVP (basis B1).⁶⁸ The effect of the solvent and a larger basis set, LACV3P**++ (designated as B2), were used for single-point calculations on the LACVP-optimized geometries. MeCN was used as the solvent with an ϵ of 37.5 and a probe radius of 2.183, as implemented in *Jaguar*. Initially, the nonhybrid functional BP86 was used to calculate the relative energies of various orientations of the copper–dioxygen complexes. However, side-on orientation of the mononuclear $[Cu^I(L^1)(O_2)]^{2+}$ complex failed to optimize at the BP86 method. With B3LYP, there were no such problems, and this functional is widely used for the study of the reaction mechanisms of copper–dioxygen complexes.⁶⁹ Spectroscopic calculations were carried out using the program ORCA.^{70,71} TDDFT calculations were performed using the B3LYP functional and a triple- ζ basis set, TZVP,⁷² on copper and all heavy atoms, with the split-valence basis set for the rest of the molecules [SV(P)]. Because of computational expense, the effect of the solvent was not considered in the TDDFT calculations. EPR calculations involved the B3LYP⁷³ functional and the CP(PPP) basis set⁷⁴ on the metal, the IGLO-III⁷⁵ basis set on the atoms directly bound to copper and the SV(P), SV/J, basis set for the rest of the atoms. Multireference configuration interaction (MRCI) calculations for the prediction of absorption spectra were carried out using the spectroscopy-oriented configuration interaction (SORCI) method.⁷⁰ Appropriate reference spaces were chosen for the complexes.⁴⁴ The initial orbitals for these calculations were chosen from BP86^{76,77} calculations, which produced quasi-restricted orbitals that were rotated to form an adequate active space. The thresholds T_{sel} , T_{pre} , and T_{nat} for these MRCI calculations were set to 10^{-6} , 10^{-5} , and 10^{-5} , respectively, and were shown to enhance the computational efficiency with a minimal loss of accuracy.⁷⁰ Resonance Raman spectra were calculated on BP86/TZVP-optimized geometries and checked for zero imaginary frequencies with the same method. The vibrational frequencies were not scaled for the complexes discussed here. If not mentioned otherwise, the relative energies reported in the paper include zero-point corrections and solvent effects.

Low-Temperature Oxygenation Experiments. The in situ generated copper(I) complexes were prepared in the appropriate solvent using $Cu^I(CH_3CN)_4(B(C_6F_5)_4)_2$,²⁶ to which was added a solution of an equimolar amount of the appropriate ligand. After standing for 5–10 min, the reaction solution was cooled (about 15 min) and molecular oxygen was bubbled through the solution for 5–15 s. THF, MeTHF, and diethyl ether (without stabilizers) were used for -80 °C measurements (cold bath = acetone, dry ice, controlled by a thermometer). For the measurements at -120 °C (cold bath = liquid nitrogen, *n*-pentane, temperature controlled by a thermometer), MeTHF was used as the solvent.

Quantitative Measurement of Molecular Oxygen Concentrations. Five reaction flasks were each charged with 0.4 g of pyrogallol and dissolved in 10 mL of deoxygenated NaOH (33% in H₂O) in a glovebox. After removal from the glovebox, 0.2, 0.4, 0.6, 0.8, and 1.0 mL of dioxygen were added via a gastight syringe and the flasks were reintroduced into the glovebox. After 18 h, 0.2 mL of the total volume was transferred to a crown-capped quartz cuvette and diluted with 1.8 mL of deoxygenated NaOH (33% in H₂O). From the calibration and using linear regression results, $y = 1.5885x - 0.0558$, $R^2 = 0.9952$ with NaOH (33% in H₂O) as the baseline. The samples were then treated similarly. The flask with the pyrogallol solution was connected to the warmed-up reaction solution and was closed using a piece of plastic tubing, before the sample flask was opened to the flask with the pyrogallol solution. The reaction solution was left stirring for 18 h, until 0.2 mL of the flask with pyrogallol had been introduced in a capped cuvette diluted with 1.8 mL of deoxygenated NaOH (33% in H₂O) and analyzed.

$[\text{Cu}^{\text{II}}(\text{L}^1)(\text{OOH})]^{2+}$. $[\text{Cu}^{\text{II}}(\text{L}^1)(\text{NCCH}_3)](\text{BF}_4)_2$ (4 mg) was dissolved in 10 mL of MeOH to give a 5.5×10^{-4} mol/L solution. This was cooled to -80°C , and 0.1 mL of NEt_3 and 0.2 mL of H_2O_2 (30 wt % in water) were slowly added. The initially blue reaction solution instantly turned to violet. This color faded away when the solution was left to warm to room temperature. At -80°C , the violet species was stable for at least 0.5 h, enabling physical measurements to be applied.

Syntheses. Caution! Although no difficulties were found using the perchlorate salts described, these are potentially explosive and need to be handled with care. Heating, especially when dry, must be avoided.

3-(4-Methoxyphenethyl)-1,5-diphenyl-7-(1,4,6-trimethyl-1,4-diazepan-6-yl)-3,7-diazabicyclo[3.3.1]nonan-9-one (L^2). A total of 1.53 mmol of (4-methoxyphenethyl)ethanamine, 3.06 mmol of a formaldehyde solution, and 0.35 mL of glacial acetic acid were mixed at 0°C in 4 mL of MeOH. The ice bath was removed, and 1.53 mmol of 1-(1,4,6-trimethyl-1,4-diazacycloheptan-6-yl)-3,5-diphenylpiperidin-4-one in 2 mL of MeOH was added. The reaction mixture was stirred for 8 h at 65°C . The solvent was removed in vacuo. The resulting oily solid was dissolved in dichloromethane, the pH was adjusted using KOH to about ~ 13 , and this solution was extracted three times with 30 mL of dichloromethane. The combined organic phases were dried with Na_2SO_4 . The solvent was removed to yield a white solid (1.00 mmol, 67%). ^1H NMR (CDCl_3 , 200.13 MHz): δ 1.12 (s, 3H, CCH_3), 2.21 (s, 6H, NCH_3), 2.23 (d, $^2J = 13.8$ Hz, 2H, $\text{CCH}_{2\text{ax}}$), 2.45 (m, 4H, CH_2CH_2), 2.75 (d, $^2J = 13.8$ Hz, 2H, $\text{CCH}_{2\text{eq}}$), 2.78 (m, 4H, $\text{NCH}_2\text{CH}_2\text{PhOMe}$), 3.07 (d, $^2J = 10.6$ Hz, 2H, $\text{CH}_{2\text{ax}}\text{NCH}_2\text{CH}_2$), 3.25 (d, $^2J = 11.0$ Hz, 2H, $\text{NCH}_{2\text{ax}}\text{C}$), 3.51 (d, $^2J = 10.6$ Hz, 2H, $\text{CH}_{2\text{eq}}\text{NCH}_2\text{CH}_2$), 3.72 (d, $^2J = 11.0$ Hz, 2H, $\text{NCH}_{2\text{eq}}\text{C}$), 3.75 (s, 3H, OCH_3), 7.14 (d, $^3J = 8.8$ Hz, 2H, $\text{CH}_{\text{ar}}\text{COCH}_3$), 7.26 (m, 12H, CH_{Ph}). ^{13}C NMR (CDCl_3 , 50.27 MHz): δ 25.10 (1C, CCH_3), 32.95 (1C, CH_2PhOMe), 48.80 (2C, NCH_3), 54.60 (1C, CCH_3), 55.23 (1C, OCH_3), 58.67 (1C, $\text{CH}_2\text{CH}_2\text{PhOMe}$), 59.41 (2C, CH_2CH_2), 60.12 (2C, CC_{Ph}), 62.11 (2C, $\text{NCH}_2\text{CC}_{\text{Ph}}$), 64.60 (2C, NCH_2CCH_3), 66.16 (2C, $\text{CH}_2\text{NCH}_2\text{CH}_2$), 113.80 (1C, $\text{C}_{\text{MeO}/\text{o}}$), 126.43 (2C, $\text{C}_{\text{Ph}/\text{p}}$), 126.85 (4C, $\text{C}_{\text{Ph}/\text{m}}$), 127.83 (4C, $\text{C}_{\text{Ph}/\text{o}}$), 129.53 (2C, $\text{C}_{\text{MeO}/\text{o}}$), 132.20 (1C, $\text{CH}_2\text{C}_{\text{MeO}}$), 143.62 (2C, OC_{MeO}), 157.92 (1C, C_{Ph}), 211.70 (1C, CO). IR (KBr-pellet): 3026, 2935, 2802, 1731, 1611, 1512, 1462, 1447, 1246, 758, 715, 698 cm^{-1} . ESI-MS (MeOH): m/z 599.21 $[\text{L}^2\text{H}(\text{CH}_3\text{OH})]^+$, 567.21 $[\text{L}^2\text{H}]^+$. Elem anal. ($\text{L}^2 \cdot 0.5\text{H}_2\text{O}$). Calcd: C, 75.10; H, 8.23; N, 9.73. Found: C, 75.18; H, 8.34; N, 9.50.

[7,7'-(1,3-Phenylenebis(methylene))bis[1,5-diphenyl-3-(1,4,6-trimethyl-1,4-diazepan-6-yl)-3,7-diazabicyclo[3.3.1]nonan-9-one] (L^3). A total of 0.18 mL (1.36 mmol) of *m*-xylylendiamine, 1.1 g of P^1 (2.8 mmol), and 0.46 mL (6.2 mmol) of a H_2CO solution (37%) were dissolved in 10 mL of THF, 10 mL of DME, and 6 mL of HOAc. The reaction mixture was stirred at 80°C for 18 h, whereupon the solvent was removed in vacuo. The resulting oily solid was suspended in 2 M HCl, and this aqueous phase was extracted once using diethyl ether. Using KOH, the pH was adjusted to ~ 13 , and the resulting solution extracted three times with 30 mL of dichloromethane. The combined organic phases were dried with Na_2SO_4 , and the solvent was removed to yield 800 mg (0.83 mmol) of product, 61%. ^1H NMR (CDCl_3 , 200.13 MHz): δ 1.22 (s, 6H, CCH_3), 2.32 (m, 16H, NCH_3 , $\text{CCH}_{2\text{ax}}\text{N}$), 2.53 (m, 8H, CH_2CH_2), 2.88 (d, $^2J = \text{Hz}$, 4H, $\text{CCH}_{2\text{eq}}\text{N}$), 3.15 (d, $^2J = 10.6$ Hz, 4H, $\text{CH}_{2\text{ax}}\text{NCH}_2\text{Py}$), 3.33 (d, 4H, $\text{CH}_{2\text{ax}}\text{NCCCH}_3$), 3.56 (d, $^2J = 10.6$ Hz, 4H, $\text{CH}_{2\text{eq}}\text{NCH}_2\text{Xyl}$), 3.75 (s, 4H, CH_2Xyl), 3.89 (d, 4H, $\text{CH}_{2\text{eq}}\text{NCCCH}_3$), 5.3 (s, 4H, CH_2Xyl), 3.70 (s, 4H, CH_2Xyl), 7.10–7.24 (m, 20H, CH_{Ph}). ESI-MS: m/z 967.63 (100%) (L^3H) $^+$. IR (KBr-pellet): 3650, 3385, 3025, 2939, 2805, 1728, 1601, 1446, 1348, 1286, 1135, 1039, 918, 751, 716, 698 cm^{-1} . Elem anal. ($\text{L}^3 \cdot \text{H}_2\text{O}$). Calcd: C, 75.57; H, 8.18; N, 11.37. Found: C, 75.64; H, 8.11; N, 11.55.

$[\text{Cu}^{\text{II}}(\text{L}^2)](\text{ClO}_4)_2$. A total of 0.09 mmol of $\text{Cu}^{\text{II}}(\text{ClO}_4)_2(\text{H}_2\text{O})_6$ was dissolved in 2 mL of CH_3CN and added to a solution of 0.09 mmol of L^2 in 2 mL of CH_3CN . After stirring at ambient temperature overnight, the resulting blue solution was treated with a diethyl ether diffusion, resulting in a green solid, 65% yield (0.06 mmol). IR (KBr pellet): 3548, 3016, 2974, 2839, 1740, 1660, 1611, 1514, 1448, 1250, 1098, 700, 624 cm^{-1} . $E_{1/2}$ (CH_3CN , 100 mV/s): -270_{irr} mV. ESI-MS (MeOH): m/z 728.08 $[\text{Cu}^{\text{II}}(\text{L}^2)(\text{ClO}_4)]^+$, 674.14 $[\text{Cu}^{\text{II}}(\text{L}^2)-$

$(\text{HCOO})^+$, 629.30 $[\text{Cu}^{\text{II}}(\text{L}^2)]^+$. Elem anal. ($[\text{Cu}^{\text{II}}(\text{L}^2)](\text{ClO}_4)_2 \cdot 3.5\text{H}_2\text{O}$). Calcd: C, 48.51; H, 5.88; N, 6.29. Found: C, 48.42; H, 5.81; N, 6.46. An X-ray structure of this complex was obtained, and it has the expected coordination geometry;^{16,25} however, the quality of the structure ($R \sim 9\%$) precludes its publication.

$[\text{Cu}_2^{\text{II}}(\text{L}^3)](\text{BF}_4)_4$. A total of 0.80 mmol of $\text{Cu}^{\text{II}}(\text{BF}_4)_2(\text{H}_2\text{O})_6$ was dissolved in 3 mL of CH_3CN and added to solution of 0.41 mmol of L^3 in 3 mL of CH_3CN . After stirring at room temperature overnight, the resulting green-blue solution was treated with a diethyl ether diffusion, resulting in a blue solid, 73% yield (0.30 mmol). Precipitation of the product could also be carried using MeOH as the solvent along with a diethyl ether diffusion. IR (KBr-pellet): 3619, 3555, 3030, 2953, 2876, 1743, 1693, 1603, 1500, 1448, 1367, 1320, 1283, 1059, 764, 699 cm^{-1} . $E_{1/2}$ (CH_3CN , 100 mV/s): -396_{ox} mV, -697_{ox} mV, -555_{red} mV. ESI-MS (MeCN): m/z 592.18 $[\text{Cu}_2^{\text{II}}(\text{L}^3)](\text{OH})(\text{F})(\text{H}_2\text{O})_2^{2+}$. Elem anal. ($[\text{Cu}_2^{\text{II}}(\text{L}^3)](\text{BF}_4)_2(\text{F})_2 \cdot 2\text{MeOH}$). Calcd: C, 56.40; H, 6.41; N, 8.10. Found: C, 56.52; H, 6.04; N, 7.86.

$[\text{Cu}^{\text{I}}(\text{L}^3)](\text{B}(\text{C}_6\text{F}_5)_4)$. A total of 0.21 mmol of $\text{Cu}^{\text{I}}(\text{B}(\text{C}_6\text{F}_5)_4)(\text{CH}_3\text{CN})_4$ and 0.10 mmol of L^3 were stirred in 5 mL of rigorously deoxygenated THF with 3 drops of CH_3CN under an oxygen-free atmosphere. After 30 min of stirring, 50 mL of deoxygenated *n*-pentane was added to precipitate the product. The solid was collected and the solvent removed in vacuo to yield 73% yield (0.07 mmol) as a yellow powder.

■ ASSOCIATED CONTENT

Supporting Information

Additional time-resolved electronic spectra, an experiment showing O_2 recovery from $[\text{Cu}^{\text{II}}(\text{L}^2)(\text{O}_2)]^+$, EPR spectra of $[\text{Cu}^{\text{II}}(\text{L}^1)(\text{NCMe})]^{2+}$ and $[\text{Cu}^{\text{II}}(\text{L}^2)(\text{OH})]^+$, CV diagrams of $[\text{Cu}^{\text{II}}(\text{L}^1)(\text{NCMe})]^{2+}$, $[\text{Cu}^{\text{II}}(\text{L}^2)(\text{OH})]^+$, and $[\text{Cu}_2^{\text{II}}(\text{L}^3)(\text{NCMe}_2)]^{4+}$, an ESI-MS experiment showing ligand oxidation of $[\text{Cu}_2^{\text{I}}(\text{L}^3)(\text{solvent})]^{n+}$ upon oxygenation, and details of the DFT calculations. This material is available free of charge via the Internet at <http://pubs.acs.org>.

■ AUTHOR INFORMATION

Corresponding Author

*E-mail: peter.comba@aci.uni-heidelberg.de (P.C.), kkarlin1@jhu.edu (K.D.K.). Fax: +49-6226-546617.

■ ACKNOWLEDGMENTS

Generous financial support by the German Science Foundation (DFG) and the University of Heidelberg (LGFG, “Molecular probes”) is gratefully acknowledged. K.D.K. acknowledges financial support from the U.S. National Institutes of Health.

■ REFERENCES

- Que, L. Jr.; Tolman, W. B. *Angew. Chem., Int. Ed.* **2002**, *41*, 1114.
- Holland, P. L.; Tolman, W. B. *Coord. Chem. Rev.* **1999**, *192*, 855.
- Kaim, W.; Rall, J. *Angew. Chem., Int. Ed.* **1996**, *35*, 43.
- Mirica, L. M.; Ottenwaelder, X.; Stack, T. D. P. *Chem. Rev.* **2004**, *104*, 1013.
- Karlin, K. D.; Kaderli, S.; Zuberbühler, A. D. *Acc. Chem. Res.* **1997**, *30*, 139.
- Schindler, S. *Eur. J. Inorg. Chem.* **2000**, 719.
- Hatcher, L. Q.; Karlin, K. D. *J. Biol. Inorg. Chem.* **2004**, *9*, 669.
- Itoh, S. *Curr. Opin. Chem. Biol.* **2006**, *10*, 115.
- Gherman, B. F.; Cramer, C. J. *Coord. Chem. Rev.* **2009**, *253*, 723.
- Kitajima, N.; Moro-oka, Y. *Coord. Chem. Rev.* **1994**, *94*, 737.
- Solomon, E. I.; Tuzcek, F.; Root, D. E.; Brown, C. A. *Chem. Rev.* **1994**, *94*, 827.
- Itoh, S. *Copper–Oxygen Chemistry*; Karlin, K. D., Itoh, S., Eds.; John Wiley & Sons: Weinheim, Germany, 2011; p 225.
- Mannich, C.; Mohs, P. *Chem. Ber.* **1930**, *B63*, 608.

- (14) Comba, P.; Nuber, B.; Ramlow, A. *J. Chem. Soc., Dalton Trans.* **1997**, 347.
- (15) Comba, P.; Kerscher, M.; Schiek, W. *Prog. Inorg. Chem.* **2007**, *55*, 613.
- (16) Comba, P.; Haaf, C.; Wadepohl, H. *Inorg. Chem.* **2009**, *48*, 6604.
- (17) Börzel, H.; Comba, P.; Katsichtis, C.; Kiefer, W.; Lienke, A.; Nagel, V.; Pritzkow, H. *Chem.—Eur. J.* **1999**, *5*, 1716.
- (18) Börzel, H.; Comba, P.; Hagen, K. S.; Katsichtis, C.; Pritzkow, H. *Chem.—Eur. J.* **2000**, *6*, 914.
- (19) Börzel, H.; Comba, P.; Pritzkow, H. *J. Chem. Soc., Chem. Commun.* **2001**, 97.
- (20) Comba, P.; Lienke, A. *Inorg. Chem.* **2001**, *40*, 5206.
- (21) Börzel, H.; Comba, P.; Hagen, K. S.; Kerscher, M.; Pritzkow, H.; Schatz, M.; Schindler, S.; Walter, O. *Inorg. Chem.* **2002**, *41*, 5440.
- (22) Comba, P.; Merz, M.; Pritzkow, H. *Eur. J. Inorg. Chem.* **2003**, 1711.
- (23) Born, K.; Comba, P.; Daubinet, A.; Fuchs, A.; Wadepohl, H. *J. Biol. Inorg. Chem.* **2007**, *12*, 36.
- (24) Comba, P.; Martin, B.; Muruganatham, A.; Straub, J., in preparation.
- (25) Comba, P.; Haaf, C.; Lienke, A.; Muruganatham, A.; Wadepohl, H. *Chem.—Eur. J.* **2009**, *15*, 10880.
- (26) Liang, H.-C.; Kim, E.; Incarvito, C. D.; Rheingold, A. L.; Karlin, K. D. *Inorg. Chem.* **2002**, *41*, 2209.
- (27) Karlin, K. D.; Cruse, R. W.; Gultneh, Y.; Farooq, A.; Hayes, J. C. *J. Am. Chem. Soc.* **1987**, *109*, 2668.
- (28) Rondelez, Y.; Séneque, O.; Rager, M.-N.; Duprat, A. F.; Reinaud, O. *Chem.—Eur. J.* **2000**, *6*, 4218.
- (29) Note that the coligand (H₂O, MeCN, MeOH, or a counterion, according to elemental analyses; see the Experimental Section) is expected to exchange in solution; i.e., for the spectra and CV in Tables 1–3 and as discussed in the text, these are assumed to be identical and correspond to the solvent.
- (30) Becker, M.; Heinemann, F. W.; Schindler, S. *Chem.—Eur. J.* **1999**, *5*, 3124.
- (31) Weitzer, M.; Schindler, S.; Brehm, G.; Schneider, S.; Hoermann, E.; Jung, B.; Kaderli, S.; Zuberbuehler, A. D. *Inorg. Chem.* **2003**, *42*, 1800.
- (32) Jacobson, R. R.; Tyeklar, Z.; Farooq, A.; Karlin, K. D.; Liu, S.; Zubietta, J. *J. Am. Chem. Soc.* **1988**, *110*, 3690.
- (33) Baldwin, M. J.; Ross, P. K.; Pate, J. E.; Tyeklar, Z.; Karlin, K. D.; Solomon, E. I. *J. Am. Chem. Soc.* **1991**, *113*, 8671.
- (34) Lee, D.-H.; Hatcher, L. Q.; Vance, M. A.; Sarangi, R.; Milligan, A. E.; Sarjeant, A. A. N.; Incarvito, C. D.; Rheingold, A. L.; Hodgson, K. O.; Hedman, B.; Solomon, E. I.; Karlin, K. D. *Inorg. Chem.* **2007**, *46*, 6056.
- (35) Lee, Y.; Lee, D.-H.; Park, G. Y.; Lucas, H. R.; Sarjeant, A. A. N.; Kieber-Emmons, M. T.; Vance, M. A.; Milligan, A. E.; Solomon, E. I.; Karlin, K. D. *Inorg. Chem.* **2010**, *49*, 8873.
- (36) Cramer, C. J.; Pak, Y. *Theor. Chem. Acc.* **2001**, *105*, 477.
- (37) Cramer, C. J.; Kinsinger, C. K.; Pak, Y. *J. Mol. Struct., Theor. Chem.* **2003**, *632*, 111.
- (38) Spuhler, P.; Holthausen, M. C. *Angew. Chem.* **2003**, *42*, 5961.
- (39) Mirica, L. M.; Vance, M.; Rudd, D. J.; Hedman, B.; Hodgson, K. O.; Solomon, E. I.; Stack, T. D. P. *Science* **2005**, *308*, 1890.
- (40) Lind, T.; Siegbahn, P. E. M.; Crabtree, R. H. *J. Phys. Chem. B* **1999**, *103*, 1193.
- (41) Siegbahn, P. E. M.; Wirstam, M. *J. Am. Chem. Soc.* **2001**, *123*, 11819.
- (42) Siegbahn, P. E. M. *J. Biol. Inorg. Chem.* **2003**, *8*, 577.
- (43) Cramer, C. J.; Wloch, M.; Piecuch, P.; Puzzarini, C.; Gagliardi, L. *J. Phys. Chem. A* **2006**, *110*, 1991.
- (44) Huber, S. M.; Shahi, A. R. M.; Aquilante, F.; Cramer, C. J.; Gagliardi, L. *J. Chem. Theory Comput.* **2009**, *5*, 2967.
- (45) Woertink, J. S.; Tian, L.; Maiti, D.; Lucas, H. R.; Himes, R. A.; Karlin, K. D.; Neese, F.; Würtele, C.; Holthausen, M. C.; Bill, E.; Sundermeyer, J.; Schindler, S.; Solomon, E. I. *Inorg. Chem.* **2010**, *49*, 9450.
- (46) Maiti, D.; Lee, D. H.; Gaoutchenova, K.; Würtele, C.; Holthausen, M. C.; Sarjeant, A. A. N.; Sundermeyer, J.; Schindler, S.; Karlin, K. D. *Angew. Chem., Int. Ed.* **2008**, *47*, 82.
- (47) Atanasov, M.; Comba, P.; Martin, B.; Müller, V.; Rajaraman, G.; Rohwer, H.; Wunderlich, S. *J. Comput. Chem.* **2006**, *27*, 1263.
- (48) Note that the transition energies are dependent on the solvent, and solvation has not been considered in our TDDFT calculations.
- (49) Note that single determinantal methods such as DFT do not allow one to compute the wave function of the superoxo complex in a single optimization.^{50,51}
- (50) Pantazis, D. A.; McGrady, J. E. *Inorg. Chem.* **2003**, *42*, 7734.
- (51) Benjamin, F.; Gherman, B. F.; Cramer, C. J. *Inorg. Chem.* **2004**, *43*, 7281.
- (52) Würtele, C.; Gaoutchenova, E.; Harms, K.; Holthausen, M. C.; Sundermeyer, J.; Schindler, S. *Angew. Chem., Int. Ed.* **2006**, *45*, 3867.
- (53) Lanci, M. P.; Smirnov, V. V.; Cramer, C. J.; Gauchenova, E. V.; Sundermeyer, J.; Roth, J. P. *J. Am. Chem. Soc.* **2007**, *129*, 14697.
- (54) Maiti, D.; Fry, H. C.; Woertink, J. S.; Vance, M. A.; Solomon, E. I.; Karlin, K. D. *J. Am. Chem. Soc.* **2007**, *129*, 264.
- (55) Kunishita, A.; Kubo, M.; Sugimoto, H.; Ogura, T.; Sato, K.; Takui, T.; Itoh, S. *J. Am. Chem. Soc.* **2009**, *131*, 2788.
- (56) Henson, M. J.; Vance, M. A.; Zhang, C. X.; Liang, H.-C.; Karlin, K. D.; Solomon, E. I. *J. Am. Chem. Soc.* **2003**, *125*, 5186.
- (57) Lee, Y.; Park, G. Y.; Lucas, H. R.; Vajda, P. L.; Kamaraj, K.; Vance, M. A.; Milligan, A. E.; Woertink, J. S.; Siegler, M. A.; Narducci Sarjeant, A. A.; Zakharov, L. N.; Rheingold, A. L.; Solomon, E. I.; Karlin, K. D. *Inorg. Chem.* **2009**, *48*, 11297.
- (58) Peterson, R. L.; Himes, R. A.; Kotani, H.; Suenobu, T.; Tian, L.; Siegler, M. A.; Solomon, E. I.; Fukuzumi, S.; Karlin, K. D. *J. Am. Chem. Soc.* **2011**, *133*, 1702.
- (59) Koder, M.; Kita, T.; Miura, I.; Nakayama, N.; Kawata, T.; Kano, K.; Hirota, S. *J. Am. Chem. Soc.* **2001**, *123*, 7715.
- (60) Ghiladi, R. A.; Huang, H.-W.; Moënne-Loccoz, P.; Stasser, J.; Blackburn, N. J.; Woods, A. S.; Cotter, R. J.; Incarnato, C. D.; Rheingold, A. L.; Karlin, K. D. *J. Biol. Inorg. Chem.* **2005**, *10*, 63.
- (61) Shearer, J.; Zhang, C. X.; Zakharov, L. N.; Rheingold, A. L.; Karlin, K. D. *J. Am. Chem. Soc.* **2005**, *127*, 5469.
- (62) Maiti, D.; Narducci Sarjeant, A. A.; Karlin, K. D. *J. Am. Chem. Soc.* **2007**, *129*, 6720.
- (63) Sanyal, I.; Mahroof-Tahir, M.; Nasir, S.; Ghosh, P.; Cohen, B. I.; Gultneh, Y.; Cruse, R.; Farooq, A.; Karlin, K. D.; Liu, S.; Zubietta, J. *Inorg. Chem.* **1992**, *31*, 4322.
- (64) Wang, D.; Hanson, G. R. *Appl. Magn. Reson.* **1996**, *11*, 401.
- (65) *Jaguar 5.5 and 6.5*; Schrödinger LLC: New York, 2005.
- (66) Becke, A. D. *J. Chem. Phys. B* **1993**, *98*, 5648.
- (67) Lee, C.; Yang, W.; Parr, R. G. *Phys. Rev. B* **1988**, *37*, 785.
- (68) Hay, P. J.; Wadt, W. R. *J. Chem. Phys.* **1985**, *82*, 270.
- (69) Güll, M.; Luis, J. M.; Sola, M.; Siegbahn, P. E. M. *J. Biol. Inorg. Chem.* **2009**, *14*, 229.
- (70) Neese, F. *J. Chem. Phys.* **2003**, *119*, 9428.
- (71) Neese, F. *Int. J. Quantum Chem.* **2001**, *83*, 104.
- (72) Schäfer, A.; Huber, C.; Ahlrichs, R. *J. Chem. Phys.* **1994**, *100*, 5829.
- (73) Holthausen, M. C.; Heinemann, C.; Cornehel, H. H.; Koch, W.; Schwarz, H. *J. Chem. Phys.* **1995**, *102*, 4931.
- (74) Neese, F. *Inorg. Chim. Acta* **2002**, *337C*, 181.
- (75) Kutzelnigg, W.; Fleischer, U.; Schindler, M. *NMR—Basic Principles and Progress*; Springer: Heidelberg, Germany, 1990.
- (76) Becke, A. D. *Phys. Rev. A* **1988**, *38*, 3098.
- (77) Perdew, J. P. *Phys. Rev. B* **1986**, *33*, 8822.